Experimental and Computational Multiphase Flow
Vol. 5, No. 4, 2023, 344–356
https://doi.org/10.1007/s42757-022-0152-8

Modeling condensing flows of humid air in transonic nozzles

Tim Hertwig[1] (✉), Tim Wittmann[1], Piotr Wiśniewski[2], Jens Friedrichs[1]

1. Institute of Jet Propulsion and Turbomachinery, Technische Universität Braunschweig, 38108 Braunschweig, Germany
2. Department of Power Engineering and Turbomachinery, Silesian University of Technology, Stanisława Konarskiego 18, 44-100 Gliwice, Poland

Abstract

The ability to accurately model condensing flows is crucial for understanding such flows in many applications. Condensing flows of pure steam have been studied extensively in the past, and several droplet growth models have been derived. The rationale for the choice of growth models for condensation in humid air is less established. Furthermore, only a few validation cases for condensation in such flows exist. This paper aims to identify existing limitations of common droplet growth laws. The Hertz–Knudsen model is compared to heat-transfer-based models by Gyarmathy and Young, using an Euler–Lagrange approach in Ansys Fluent. For this, an adaption for Young's growth law is introduced, allowing its application in condensation of different gas mixtures. The numerical model has been validated and applied to flows in nozzles and turbines in previous publications. The accuracy of the droplet growth models is investigated in transonic nozzle test cases. A case with pure steam and a case with humid air at two different humidity values are considered. Finally, the influence of humidity, Knudsen number, and droplet radius on the growth rate of each model is shown analytically. Flows at lower humidity values with longer condensation zones are shown to benefit from the higher sensitivity of the Hertz–Knudsen model to the mass fraction of water vapor in the flow. Heat-transfer-based models tend to overestimate condensation in such flows. However, the ability to empirically adapt the growth model by Young and its applicability in different Knudsen numbers results in good agreement with validation data over a wide range of cases.

Keywords

condensation
transonic nozzles
droplet growth
CFD
humid air

Article History

Received: 5 April 2022
Revised: 21 September 2022
Accepted: 24 November 2022

Research Article

1 Introduction

Due to its importance in steam turbines, condensation in flows of pure steam has been studied extensively in the past (Bakhtar, 2004). Due to the increasing importance of applications with condensing flows of humid air, such as fuel cells (Wittmann et al., 2021c), aerospace intakes (Young, 1995), electricity production (Roumeliotis and Mathioudakis, 2006), and compressor rotors (Wiśniewski et al., 2022b), accurate models are necessary. Such models are usually based on equations derived for condensation in pure steam. Homogenous condensation, i.e., condensation without the presence of suspended particles, relies on the formation of stable nuclei. The fundamental theory for this process was derived by Frenkel (1955). Over the past decades, multiple corrections have been introduced. A review on classical nucleation theory for homogenous nucleation was published by Bakhtar et al. (2005).

Stable nuclei subsequently provide the surface for further condensation. This process is modeled using growth models, which are the main focus of this study. As the droplets grow, their Knudsen number decreases sharply. As a result, condensation not only takes place in the free-molecular regime, but crosses into the transitional regime and, depending on the case, even into the continuous regime. Thus, the growth model has to accurately take into account the physical behavior of the condensation process in the respective regime. Simpler models like the Hertz–Knudsen model rely on molecular kinetic theory by balancing the condensing and evaporating fluxes and are thus only valid in the free-molecular regime (Hill, 1966).

A different approach was taken by Gyarmathy (1962).

✉ t.hertwig@tu-braunschweig.de

Nomenclature

Latin letters

C_C	Cunningham correction factor
C_D	Drag coefficient
ΔT	Subcooling (K)
f_σ	Correction factor of the planar surface tension
h_{fg}	Latent heat (J/(kg·K))
J_{CL}	Classical nucleation rate ($m^{-3}·s^{-1}$)
J_{NISO}	Nucleation rate with non-isothermal correction by Kantrowitz ($m^{-3}·s^{-1}$)
k_B	Boltzmann constant (J/kg)
Kn	Knudsen number
l	Mean free path (m)
m	Molecular mass (kg)
Pr	Prandtl number
q_c	Condensation coefficient
R	Gas constant (J/kg)
r	Droplet radius (m)
r_{crit}	Critical radius (m)
Re	Reynolds number
S	Super-saturation ratio
T	Temperature (K)
t	Time (s)
w	Mass fraction
x	Distance from nozzle throat (m)

Greek letters

α	Factor in Young's growth law
α_r	Heat transfer coefficient ($W/(m^2·K)$)
β	Factor in Young's growth law
γ	Ratio of specific heats
λ	Conductivity ($W/(m^2·K)$)
μ	Dynamic viscosity (kg/(m·s))
ν	Factor in Young's growth law
φ	Relative humidity
Φ	Non-isothermal correction factor
ρ	Density (kg/m^3)
σ	Surface tension (kg/m^2)

Abbreviations

IAPWS	International Association for the Properties of Water and Steam
IWSMP	International Wet Steam Modeling Project
SUT	Silesian University of Technology

Subscripts

g	Vapor phase
H_2O	Water species
l	Liquid phase
p	Particle
sat	Saturation state
t	Stagnation state

His growth model assumes that the process of condensation is limited by the rate at which heat can be carried away from the droplet. By introducing a corrected heat-transfer coefficient dependent on the Knudsen number, Gyarmathy's growth model transitions between continuous heat transfer and free-molecular heat transfer, thus allowing the modeling of condensation in all regimes (Moore and Sieverding, 1976). This approach was further refined and corrected by Young (1982), primarily to improve results at low pressures. An extensive overview of the different growth models and a comparison between different numerical approaches from a large number of institutions can be found in the results of the International Wet Steam Modeling Project (IWSMP) (Starzmann et al., 2018). The IWSMP found considerable uncertainties in the available models and showed that the empirical nature of the growth models in particular requires rigorous validation. However, while the IWSMP compared a wide variety of models, including Euler–Lagrange and Euler–Euler approaches with different growth laws, it only investigated flows of pure steam.

Condensation models are typically validated with measurements in transonic wet steam nozzles. Common examples include the Moses and Stein (Moses and Stein, 1978) and Moore nozzles (Moore and Sieverding, 1976). However, only little experimental data exists for condensation in humid air. Dykas et al. (2017) obtained pressure measurements in two different nozzles at two humidity conditions each.

The multiphase can be numerically modeled with either an Euler–Euler or an Euler–Lagrange approach. White (2003) provides a comparison between the two methods. While the Euler–Euler approach provides good computational efficiency due to better parallelizability, the Euler–Lagrange approach allows the resolution of the discrete droplet spectrum. Additionally, multiple droplet sizes per cell can exist (Hughes et al., 2016). Nonetheless, the vast majority of investigations uses an Euler–Euler approach for modeling condensation (Gerber and Kermani, 2004; Wróblewski et al., 2009; Starzmann et al., 2012; Chandler et al., 2014; Grübel et al., 2015). For this investigation, an Euler–Lagrange approach is used, which has been introduced and validated in more detail in Wittmann et al. (2021a) and has been applied to condensation in fuel cell turbocharger turbines with humid air in previous publications (Wittmann et al., 2021b, 2021c). Similar Euler–Lagrange models have been

used to model condensation in radial turbines (Schuster et al., 2018a, 2018b) and steam turbines (Gerber, 2002; Fakhari, 2006; Sasao et al., 2013). A review on the use of Euler–Lagrange models in different applications was published by Subramaniam (2013).

Recent investigations analyzed both homogenous and heterogeneous condensation in humid air in both internal and external flows (Dykas et al., 2018, 2020; Wiśniewski et al., 2020a, 2020b). Wisniewski et al. recommended a Hertz–Knudsen model for homogenous condensation in humid air. However, their single-fluid approach did not allow any analysis of spectrum statistics (Wiśniewski et al., 2022a). Moreover, they introduced a blending model, which applies a linear interpolation between the Hertz–Knudsen and the Fuchs–Sutugin models depending on the Knudsen number.

Since the growth model is of particular importance for the accuracy of a condensation model, this study aims to investigate the choice of such a model for modeling condensation in humid air. For this, transonic nozzles for pure steam as well as humid air with available measurements of pressure and droplet radius are used to compare the predictions of different models. Additionally, the necessary adaptations to the growth model by Young to allow its application to humid air and other fluids are outlined. Finally, the sensitivity of the different models to changes in droplet radius and humidity is examined.

2 Theory

The nozzles investigated here are converging–diverging nozzles, in which the flow is accelerated to supersonic speeds. Transonic nozzles are used for validation of condensation models as the flow is simpler than that of a turbine and can be designed to be steady and nearly 1D, while still retaining the subcooling conditions present in real turbines (Starzmann et al., 2018). Figure 1 shows the development of common flow parameters in such a nozzle.

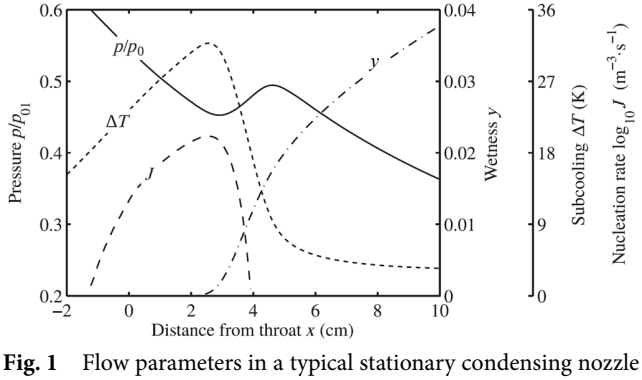

Fig. 1 Flow parameters in a typical stationary condensing nozzle (Starzmann et al., 2018).

During acceleration, the pressure decreases in the direction of the flow, and thus the saturation of the flow with water vapor increases. Once the flow is fully saturated, it subcools, and the subcooling $\Delta T = T_{sat} - T_g$, where T_{sat} and T_g are the saturation temperature and the temperature of the gas flow, respectively. When the subcooling is large enough for a sufficient number of stable clusters to form, the nucleation rate increases sharply. The point with maximum subcooling is known as the Wilson point. Subsequently, the droplets grow as more vapor condenses and the wetness y increases. The latent heat released by the condensation raises the temperature of the surrounding gas and leads to a decrease in subcooling, thus bringing the flow back to an equilibrium state. The latent heat additionally leads to a characteristic rise in static pressure, that is subsequently equalized due to the ongoing expansion. (Starzmann et al., 2018). The rate at which stable nuclei form in a specific volume is modeled with the classical homogenous nucleation rate, commonly attributed to Frenkel (1955):

$$J_{CL} = q_c \frac{\rho_g \rho_v}{\rho_l} \sqrt{\frac{2\sigma_g}{\pi m_{H_2O}^3}} \exp\left(-\frac{4\pi\sigma_g}{3k_B T_g} r_{crit}^2 \right) \tag{1}$$

with the condensation coefficient q_c, the densities ρ_g, ρ_v, and ρ_l of the gas, vapor, and liquid phases, respectively, the planar surface tension of water σ_g, the molecular mass of water m_{H_2O}, the Boltzmann constant k_B, the temperature of the gas phase T_g, and the critical radius

$$r_{crit} = \frac{2\sigma_g}{\rho_l R T_g \ln S} \tag{2}$$

where R and $S = p/p_{sat}$ are the specific gas constant and the super-saturation, respectively. The critical radius is the smallest radius at which nucleated clusters are stable, i.e., above which continued growth of the droplet leads to decrease of the free energy in the system (Bakhtar et al., 2005). Since the classical nucleation rate neglects the temperature gradient between the droplets and the surrounding flow, it is corrected using the commonly applied non-isothermal correction by Kantrowitz (1951). This results in the corrected nucleation rate

$$J_{NISO} = \frac{J_{CL}}{1+\Phi} \tag{3}$$

with the non-isothermal correction factor

$$\Phi = 2\frac{\gamma-1}{\gamma+1}\frac{h_{fg}}{RT_g}\left(\frac{h_{fg}}{RT_g} - \frac{1}{2}\right)$$

Here, h_{fg} is the latent heat and γ the ratio of specific heats, which reduces J_{CL} by a factor of 50–100. The Knudsen number Kn is defined as the ratio between the mean free

path $\bar{l}$ and the diameter of the droplet $2r$, where

$$\bar{l} = 1.5\mu\frac{\sqrt{RT_g}}{p_g} \tag{4}$$

with the dynamic viscosity μ and the pressure of the gas phase p_g.

In general, two different approaches can be used to model the droplet growth rate. The first is employing equations derived from molecular kinetic theory by balancing the mass and energy fluxes away from and to the droplet. A commonly used growth law is the Hertz–Knudsen equation

$$\frac{dr}{dt} = \frac{q_c}{\rho_f}\left(\frac{p_{H_2O}}{\sqrt{2\pi RT_g}} - \frac{p_{sat,l}}{\sqrt{2\pi RT_l}}\right) \tag{5}$$

where p_{H_2O} and $p_{sat,l}$ are the partial pressure of the water vapor and the saturation pressure of the droplet, respectively. T_l is the temperature of the liquid phase. For pure steam flows, the refined version by Hill (1966) is often employed. Hill's law differentiates between the mass and energy fluxes to and from the droplet that condense, evaporate, and are reflected. As terms are neglected based on the assumption of pure steam, this law is not further analyzed here.

The second approach is based on the assumption that the rate at which latent heat can be transferred away from the droplet limits the rate of condensation, which was introduced by Gyarmathy (1962). He introduced the corrected heat transfer coefficient α_r dependent on the Knudsen number:

$$\alpha_r = \frac{\lambda_g}{r}\frac{1}{1+3.18Kn} \tag{6}$$

with the thermal conductivity of the vapor phase λ_g and the droplet radius r. The second term interpolates between the continuous and the free-molecular regimes. It becomes one for small Kn, and α_r follows the values described by Chambre and Schaaf (2017) for large Kn. The resulting growth law by Gyarmathy (1962) is

$$\frac{dr}{dt} = \frac{\alpha_r}{\rho_l h_{fg}}\left(T_l - T_g\right) = \frac{\lambda_g\left(T_l - T_g\right)}{\rho_f h_{fg} r(1+3.18Kn)} \tag{7}$$

This was later expanded and corrected by Young (1982), yielding Young's growth law:

$$\frac{dr}{dt} = \frac{\lambda_g\left(1-\frac{r_{crit}}{r}\right)\Delta T}{\rho_l h_{fg} r\left[\frac{1}{1+2\beta Kn} + 3.78\,(1-\nu)\frac{Kn}{Pr}\right]} \tag{8}$$

where β is an empirical factor describing the boundary of the free-molecular layer around the droplet, and Pr is the Prandtl number of the vapor phase. For this study β is set to $\beta = 0$, which is a common assumption as the influence of β is small compared to other parameters. The factor ν is defined as

$$\nu = \frac{RT_{sat}}{h_{fg}}\left(\alpha - 0.5 - \frac{2-q_c}{2q_c}\frac{\gamma+1}{2\gamma}\frac{c_{pg}T_{sat}}{h_{fg}}\right)$$

with the second empirical factor α describing the relationship between the condensation and evaporation coefficients. Since the factor of 3.78 in Eq. (8) was derived for pure steam, a correction is introduced here, following the original derivation by Gyarmathy as explained in Moore and Sieverding (1976). Assuming a perfect thermal accommodation of the colliding molecules, the factor is corrected, yielding

$$3.78\frac{Kn}{Pr} \Rightarrow 2\frac{\sqrt{8\pi}}{1.5\,Pr}\frac{\gamma}{\gamma+1}Kn \approx 6.684\frac{\gamma}{\gamma+1}\frac{Kn}{Pr} \tag{9}$$

Thus, Young's growth law can be modified to read

$$\frac{dr}{dt} = \frac{\lambda_g\left(1-\frac{r_{crit}}{r}\right)\Delta T}{\rho_l h_{fg} r\left[\frac{1}{1+2\beta Kn} + 6.684\frac{\gamma}{\gamma+1}(1-\nu)\frac{Kn}{Pr}\right]} \tag{10}$$

By using the ratio of specific heats γ of the particular gas mixture, this equation allows the modeling of the droplet growth, even if other gases such as air are present in the mixture. As shown in Fig. 2, the influence on the growth rate is quite small. Nonetheless, the accuracy of the results might still be affected in the cases with strong condensation, particularly in higher humidity condition. In general, the correction reduces the calculated droplet growth rate. In the cases with pure steam, the equation becomes identical

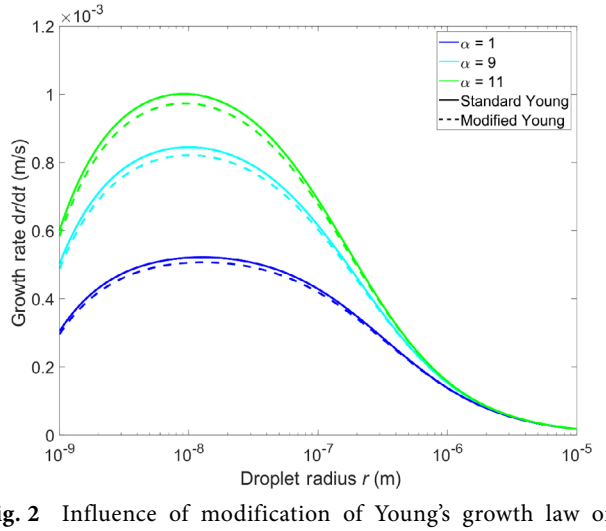

Fig. 2 Influence of modification of Young's growth law on growth rate in dependence of droplet radius with $\Delta T = 35$ K, $p_g = 40{,}000$ Pa, and an H_2O mass fraction of $w_{H_2O} = 0.8\%$.

to the original growth law. Additionally, Fig. 2 shows the non-linear increase in predicted growth rate when increasing α.

3 Methodology

To analyze the influence of the choice of growth law, different nozzle validation cases are used. This section introduces the geometries and the numerical approach.

3.1 Cases

The first nozzle case is case 252 introduced by Moses and Stein (1978), which shall hereinafter be called Moses 252. Its geometry has a throat height of 10 mm, an inlet stagnation pressure of $p_t = 40{,}050$ Pa, and an inlet stagnation temperature of $T_t = 374.3$ K. The pressure measurements along the centerline and droplet size data obtained via light scattering were given in the original paper by Moses and Stein (1978), processed by Young (1982) and provided by the organizers of the IWSMP (Starzmann et al., 2018). The provided datasets are shown in Fig. 4 in black. Figure 3 shows contours of static pressure for Moses 252. As this case was created for pure steam, the validation is carried out accordingly. Moreover, since radius measurements are not available for the cases with humid air, only this case can be used to estimate the accuracy of the different growth

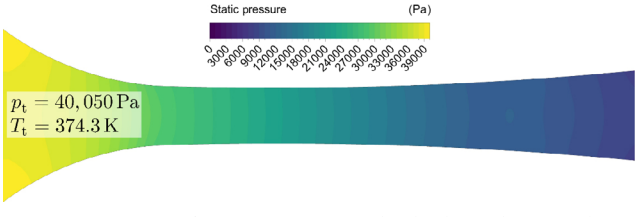

Fig. 3 Contours of static pressure and inlet boundary condition for Moses 252.

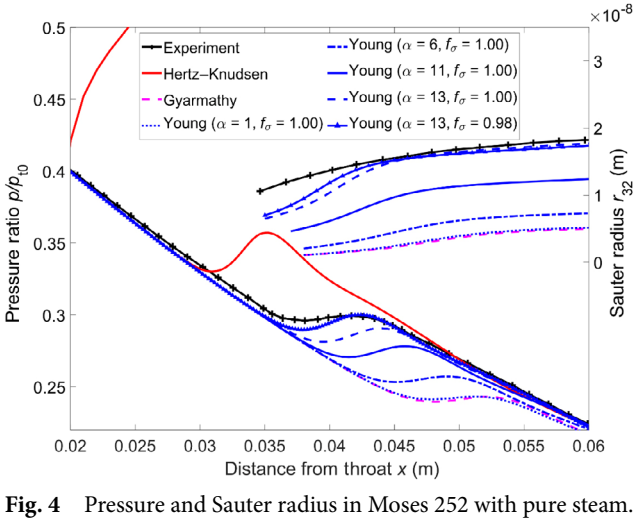

Fig. 4 Pressure and Sauter radius in Moses 252 with pure steam.

laws in terms of both radius and pressure. The results of the validation are shown in Fig. 4. It is obvious that the predictions vary significantly between the different models. In this case, Gyarmathy's growth law aligns with Young with $\alpha = 1$. This differs from the observation of the IWSMP, where the growth rate calculated with Gyarmathy's growth law is estimated to roughly align with Young at $\alpha = 4$. However, the corresponding growth rates for this estimation were determined for $T = 15$ K and $p = 25$ kPa, which is not identical to the properties at the Wilson point of Moses 252. Since the growth laws exhibit different sensitivities to thermodynamic properties of the flow, it is not possible to observe a clear relationship between them, as will also be shown later. Furthermore, α can be observed to strongly impact both the location and the amplitude of the pressure peak, as well as the mean radii. Due to the uncertainties connected to condensation modeling, an empirical calibration is commonly carried out.

With the current model, the best fit is achieved with $\alpha = 13$ and a correction of the planar surface tension with a factor of $f_\sigma = 0.98$. The latter is commonly applied to account for the surface tension of a curved surface. As can be seen in Fig. 4, this adjustment leads to an upstream shift of the condensation onset and an increase in the pressure peak due to increased nucleation and growth rates. However, as this factor introduces an additional degree of freedom and further uncertainty, it is set to $f_\sigma = 1.0$ for the following investigations. All heat-transfer-based models underestimate the condensation in this case. The molecular kinetic Hertz–Knudsen model, on the other hand, overestimates both pressure and Sauter radius r_{32}. Due to its lack of empirical factors, an improvement in accuracy cannot be achieved with this model.

The second geometry is a circular nozzle with a throat diameter of 0.02 m and a diameter of the curvature of 0.1 m, which has been provided by the Silesian University of Technology. Pressure measurements along the centerline for two cases with humid air introduced by Dykas et al. (2017) are available. Both cases have inlet stagnation pressures and temperatures of $p_t = 98{,}900$ Pa and $T_t = 297$ K, respectively. The first case, hereinafter called SUT43, has a relative humidity at the inlet of $\varphi = 43\%$, whereas the second case, hereinafter called SUT68, is set to an inlet humidity of $\varphi = 68\%$. These humidity values correspond to mass fractions of water vapor of $w_{H_2O} \approx 0.0080$ and $w_{H_2O} \approx 0.0129$, respectively. Figure 5 shows the pressure contours for SUT68. A condensation shock occurs shortly after the throat. This is not present in SUT43.

3.2 Numerical approach

The numerical simulations for this study are conducted

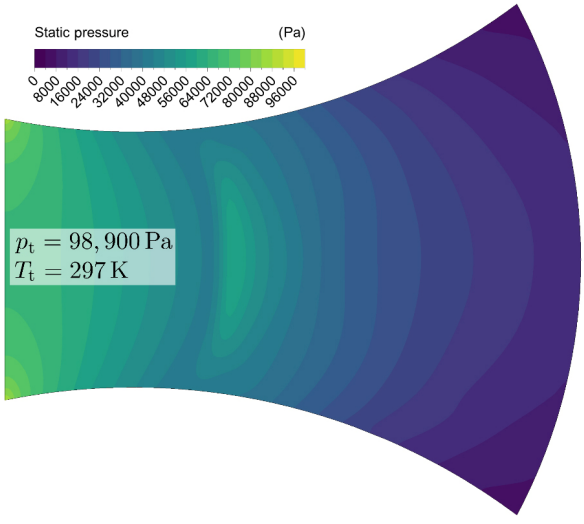

Fig. 5 Contours of static pressure and inlet boundary condition for SUT68.

using an Euler–Lagrange approach implemented in Ansys Fluent with user-defined functions in the Discrete Particle Model. An SST k–ω turbulence model with viscous heating is applied to the continuous phase. The discrete droplets are modeled as parcels initialized in the center of the respective cell if $J \geq 1\times10^{12}\,\mathrm{m}^{-3}\cdot\mathrm{s}^{-1}$. This threshold is applied to speed up the calculation. However, compared to other researchers, such as Schuster et al. (2018a) and Gerber (2002), a smaller minimum nucleation rate is used here, as it was found to be required for a sufficient resolution of the condensation effects.

The droplet parcels are nucleated at the temperature and velocity of the surrounding vapor, as well as the local critical radius, and consist of the corresponding number of droplets nucleated per second in the respective cell. Using the velocity field of the continuous phase, each parcel's trajectory is then integrated, taking into account the slip between the phases. Both the influence of the thermophoretic force and the drag are considered. The latter is calculated via the correlation by Schiller and Naumann (1935), which reads

$$C_D = C_C \frac{24}{Re_p}\left(1+0.15Re_p^{0.687}\right) \tag{11}$$

with the particle Reynolds number Re_p, and the correction factor by Cunningham (1910) for particles at large Knudsen numbers Kn, which reads

$$C_C = \frac{1}{1+2.53Kn} \tag{12}$$

Finally, the droplet growth is calculated along each trajectory, and sources for momentum, mass, and energy exchange between the phases are added to the governing equations of the vapor phase. The quasi-steady droplet temperature of the droplet for the growth laws by Young and Gyarmathy is calculated with the approximation by Gyarmathy (1962):

$$T_l - T_g = \Delta T\left(1-\frac{r_{crit}}{r}\right) \tag{13}$$

As the Hertz–Knudsen model reacts quite sensitively to the introduction of this approximation, the droplet is assumed to be isothermal for the calculation with this model. For Gyarmathy, on the other hand, it is strictly necessary as no droplet growth is predicted otherwise, since no heat transfer can occur. The influence of this is analyzed later. A schematic diagram of the numerical approach is shown in Fig. 6.

The thermodynamic properties used for nucleation and condensation are calculated using the equations from IAPWS R7-97 (2012). All properties of the Euler phase are calculated using fitted real gas equations. For steam, the relations were taken from Adam (1996), while the equations for air were provided by the Silesian University of Technology. Relatively strong under relaxation of the discrete phase sources and pseudo-transient under relaxation are applied to achieve numerical stability.

Additionally, a fully analytical growth model is implemented in MATLAB, also using the IAPWS IF-97 equations. This is used to produce the figures depicting

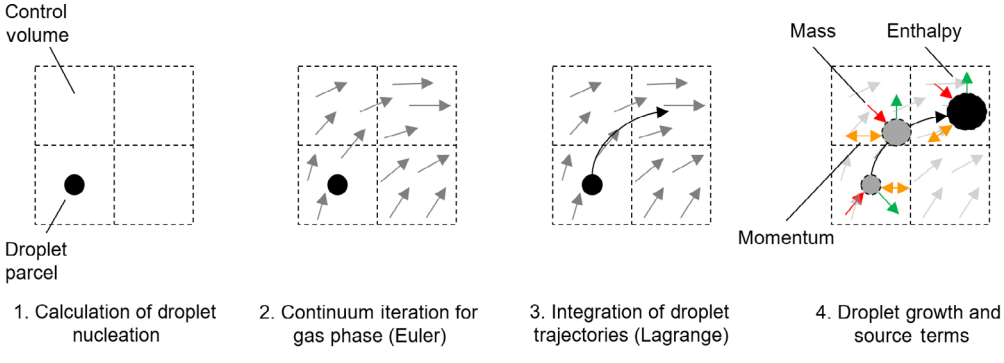

Fig. 6 Schematic visualization of the Euler–Lagrange approach.

the calculated droplet growth rates dependent on Knudsen number or droplet radius.

As the droplets in the SUT nozzle supercool below the freezing point in both cases, attention needs to be paid to the validity of the equations of state. Both nucleation and droplet growth are sensitive to the accuracy of the density of liquid water in particular. Thus, the equations from the G12-15 guidelines for supercooled water by IAPWS G12-15 (2015) are used. The calculation switches to this formulation below the triple point. As supercooled water is stable in two states, the mole fraction of the low-density structure has to be determined numerically. For this, a Brent solver is used, which finds the root of a given problem by using specified minimum and maximum values (Brent, 1973). The boundaries for the root-finding algorithm are calculated via the equations given in G12-15.

3.4 Mesh sensitivity analysis

To analyze the mesh resolution required by the condensation model, three meshes are created for Moses 252. The coarsest and finest meshes consist of about 15,000 and 66,000 cells, respectively. Figure 7 shows the mesh convergence in terms of static pressure and Sauter radius, using the best fitting growth law by Young with $\alpha = 13$, $\beta = 0$, and a correction of the planar surface tension of $f_\sigma = 0.98$ with pure steam. It is obvious that full convergence in terms of both properties is achieved even with the coarsest mesh. The droplet spectrum shown in Fig. 8 is far more sensitive to the mesh resolution.

At the sampling location near the nozzle exit, the discrepancies introduced by the coarsest mesh add up. As the droplets are lumped together as parcels, larger cell sizes increase the number of droplets per parcel and thus reduce the variety of droplet sizes that can be modeled. This effect results in the more discrete peak at larger radii, with fewer smaller droplets being sampled at smallar radii.

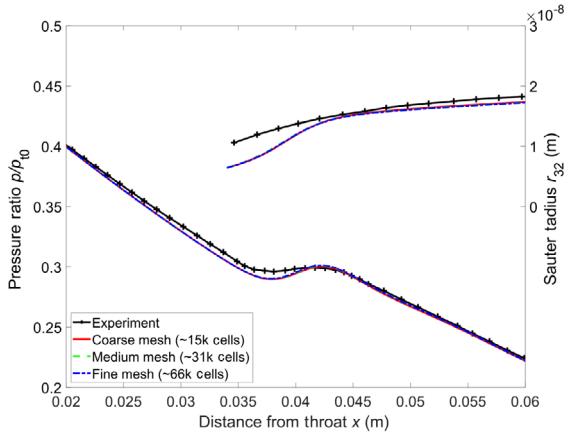

Fig. 7 Comparison of pressure and Sauter radius for different mesh resolutions with pure steam in Moses 252.

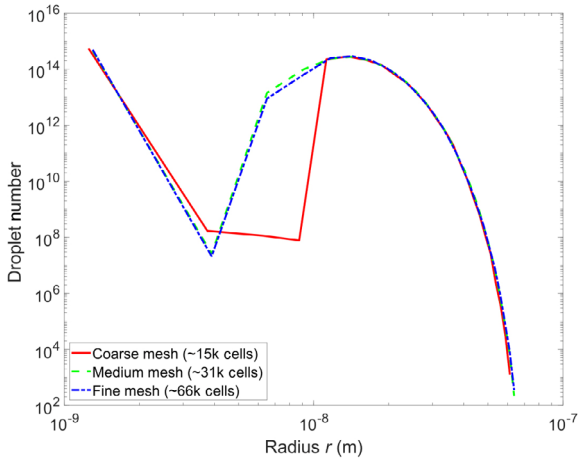

Fig. 8 Comparison of droplet spectra for different mesh resolutions with pure steam in Moses 252 at $x = 0.06$ using Young's growth law with $\alpha = 13$ and $f_\sigma = 0.98$.

Nonetheless, the main peak at larger radii is sufficiently captured even with the coarsest mesh. A noteworthy effect is the large number of droplets with radii near the critical radius. These are the droplets that would normally evaporate and are thus not able to grow.

Additional discrepancies might have been introduced by the binning process used to generate the continuous spectrum from a discrete number of droplets, and the main contribution to the exchanged heat stems from the largest droplets, since these are the droplets that had the longest time to grow and were thus mainly nucleated at or shortly downstream of the Wilson point. Since the surface area available for condensation increases quadratically with radius, the disproportionate contribution of the largest droplets is even more distinct. As for the main peak in the droplet spectrum, the Sauter radius and the static pressure are sufficiently captured with the coarsest mesh consisting of about 15,000 cells, which are selected for the following analysis. Additionally, the coarsest mesh provides the best computational efficiency. As each parcel has to be tracked individually in an Euler–Lagrange approach, the computational demand increases considerably with finer grids.

4 Results

The results of the simulations and the analytical calculations can be assessed to identify important influencing factors for the selection of a suitable growth model. In particular, the accuracy of the models over a variety of Knudsen numbers is analyzed.

4.1 Influence of Gyarmathy approximation

To analyze the influence of the droplet growth model, the influence of the Gyarmathy approximation has to be assessed,

as it is neglected for calculations with Hertz–Knudsen. As can be seen in Fig. 9, Young's growth model is insensitive to changes in the droplet temperature. This is due to the fact that Young uses the subcooling of the vapor phase, as opposed to the difference between the temperatures of the liquid and vapor phases used by Gyarmathy.

Gyarmathy's growth law on the other hand strictly requires a temperature difference, since it calculates the heat transfer at the interface between the droplet and the surrounding vapor. As such it only predicts droplet growth if the approximation is used. In that case, the predicted growth rate is almost identical to that predicted with Young using $\alpha = 1$, which is in line with the pressure and Sauter radius seen in Fig. 4. Identically, the growth rate predicted by Hertz–Knudsen is considerably larger than that predicted using the other models, which becomes obvious as an overestimation of pressure and particularly droplet radius in Fig. 4. Moreover, the Gyarmathy approximation leads to a reduction in the predicted growth rate.

All growth laws predict decreasing growth rates with increasing Knudsen number. While the decrease is roughly linear with both Gyarmathy and Hertz–Knudsen, the slope of the curve decreases at small Knudsen numbers with Young, particularly with larger α. This is an effect of the interpolation between the free-molecular and continuous regime, which is also present with Gyarmathy, but becomes more pronounced with larger α in Young. As Fig. 9 was generated by varying the pressure, while the temperature is only indirectly influenced via the saturation pressure, the change in heat transfer due to the flow regime dominates the growth rate. As the flow approaches the continuous regime when the droplets grow, the heat transfer with the surrounding vapor is no longer inhibited by the distances necessary for molecular collisions. Therefore, the rate of heat transfer and accordingly the growth rate approach a plateau if the temperature difference remains almost constant.

With humid air, the influence of the Gyarmathy approximation does not change. The predicted growth rates, particularly with Hertz–Knudsen, however, shift downwards with lower H_2O mass fractions, which will be shown later.

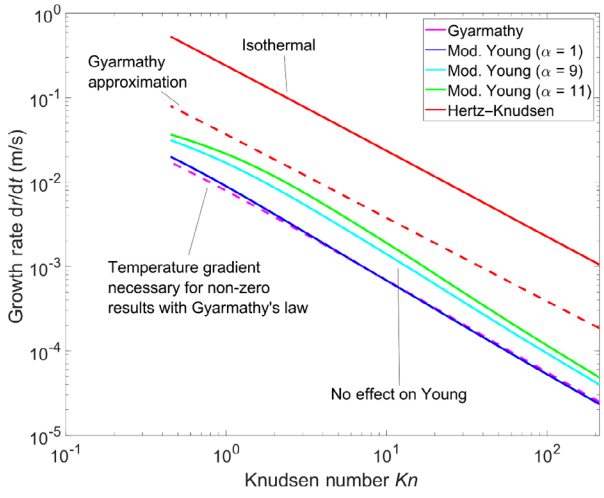

Fig. 9 Influence of Gyarmathy approximation on droplet growth rate different growth laws with a constant subcooling of $\Delta T = 30$ K and droplet radius of $r = 10$ nm at $w_{H_2O} = 1$.

4.2 Influence of Knudsen number

The result of changing the Knudsen number in the flow is shown in Fig. 10. For this, Moses 252 was simulated with humid air and a vapor mass fraction of 10% at the inlet. Starting at the original temperature, the inlet temperature was successively lowered to assess the influence on the flow and the Knudsen number. The case shown here was conducted with Young at $\alpha = 11$. However, the initial Knudsen number is only an effect of the location of the Wilson point and the critical radius at that location.

Smaller temperatures increase the subcooling and thus shift the onset of nucleation upstream. Since expansion is less progressed the further upstream the Wilson point is located, the initial Knudsen number is smaller. As seen earlier, this results in stronger droplet growth. This decreases the distance necessary for the subcooling to be reversed, results in the nucleation of fewer droplets, and leads to a smaller Knudsen number shortly after the Wilson point. In this

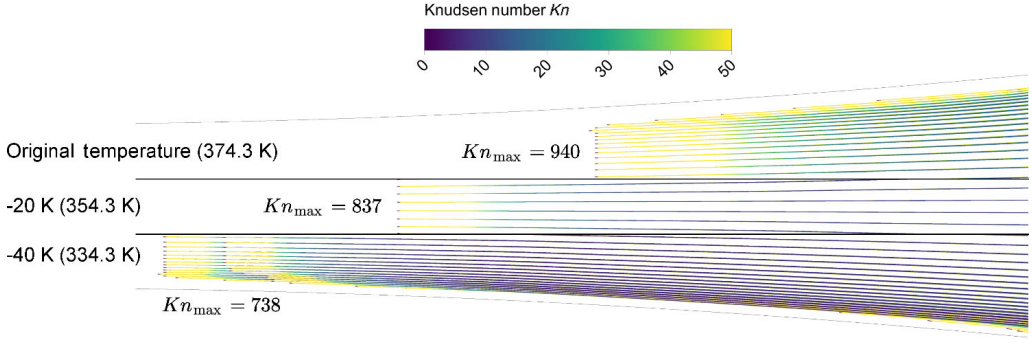

Fig. 10 Influence of temperature on Knudsen number in Moses 252 with humid air and $w_{H_2O} = 0.1$.

example, the influence of the flow regime is less pronounced, as the temperature changes are more extreme compared to the isolated example in Fig. 9.

4.3 Behavior of growth models

Figure 11(a) shows the predictions of the different growth models for the SUT nozzle at 43% relative humidity against experimental results. As measurements of the droplet radius are not available, it is not shown. In contrast to the strong overestimation of the condensation by Hertz–Knudsen model in Fig. 4, Hertz–Knudsen model predicts less condensation than the other growth laws, and shows the best agreement with the data. However, the onset of the pressure peak is located slightly behind the measured location, indicating that the initial growth of the first droplets is underestimated.

The heat-transfer-based models on the other hand overestimate the amplitude of the pressure peak. This is particularly evident with Young's growth law at $\alpha = 11$, where the large droplet growth rates shift the onset of the peak upstream, while also increasing its amplitude. Additionally, the modification of Young's growth law is too small to be visible in this graph. As observed before, Gyarmathy's growth law yields similar results compared to Young. As opposed to the overlap with Young at $\alpha = 1$ in Fig. 2, however, its prediction is roughly similar to Young with $\alpha = 6$ in this case. The discrepancies between the predictions with pure steam and humid air can be explained by the surrounding air cooling the droplets, while acting as an inert gas with regard to the condensation itself. This effect is better captured with a molecular-kinetic growth model like Hertz–Knudsen, which only considers the partial pressure of the vapor.

The Knudsen number used in the heat-transfer-based models, on the other hand, has to be calculated with the static pressure of the mixture. This results in a droplet growth rate that assumes the whole gas mixture to take part in the condensation. However, if the mean free path were to be calculated via the partial pressure instead, heat transfer via collisions with air molecules would be neglected, thus strongly underestimating the growth rate.

The accuracy of the pressure prediction is less affected by air when the humidity is increased. This can be seen in Fig. 11(b) in the SUT nozzle with 68% relative humidity at the inlet. While the mass fraction of water vapor is still small, the nucleation rate is increased drastically compared to the case with 43% relative humidity. The resulting condensation shock leads to a far shorter condensation zone, with all growth laws predicting large growth rates. As the droplets grow more over a shorter distance and thus travel through less cooling medium, the influence of the surrounding air on the heat transfer away from the droplets is less pronounced.

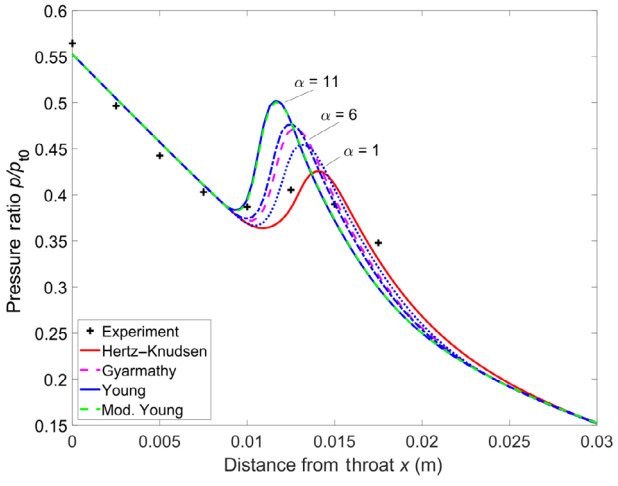

(a) SUT43

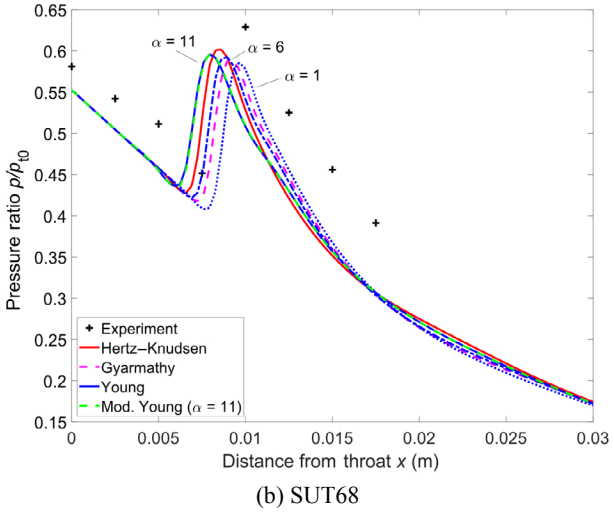

(b) SUT68

Fig. 11 Pressure in SUT nozzle for different growth laws.

Thus, the growth laws predict similar pressure peaks. Since re-evaporation of droplets occurs behind the condensation shock, which is not modeled, the agreement with the measurements is worse than with lower humidity values. Again, the modification of Young's growth law does not affect the pressure prediction. Moreover, the upstream shift of the onset of condensation and the increase in amplitude of the pressure peak with larger α is also reflected here, albeit less pronounced.

The differences between the two cases at different humidity values become more evident in the droplet spectra shown in Figs. 12(a) and 12(b). The spectra were sampled at $x = 0.03$ m near the outlet, which most resembles the asymptotic state approached by the spectra once equilibrium is reached. Interestingly, both the maximum droplet radius and droplet number change only little between the cases with the heat-transfer-based models. The maximum radius predicted with Hertz–Knudsen, however, increases between the cases. As the significant growth of droplets sets in later

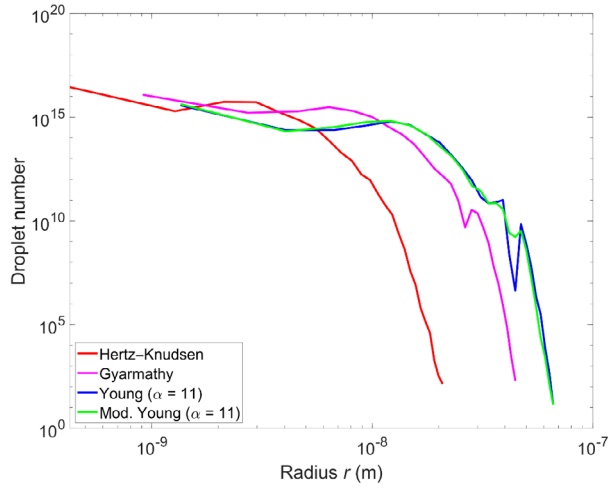

(a) SUT43

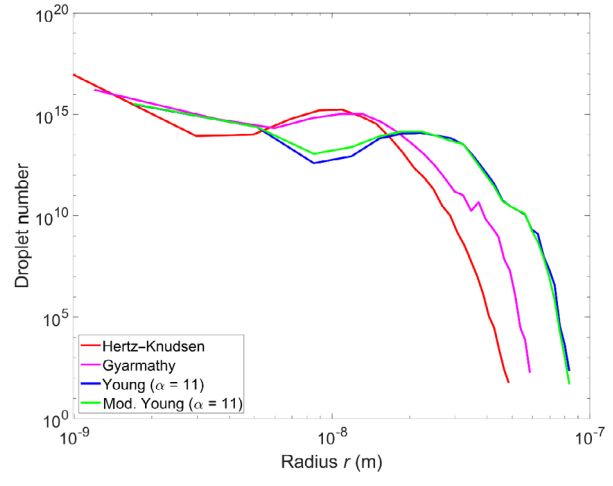

(b) SUT68

Fig. 12 Comparison of droplet spectra between different growth laws at $x = 0.03$ m.

with Hertz–Knudsen and Gyarmathy compared to Young at $\alpha = 11$, more droplets are nucleated but less growth per droplet occurs at $\varphi = 43\%$. However, the spectra at this humidity are smooth with almost constant droplet numbers over all radii, with a steep drop-off at the maximum radius. This is a result of the longer nucleation zone and the slower release of latent heat due to smaller growth rates. At $\varphi = 68\%$ on the other hand, a peak in droplet number occurs shortly before the drop-off. This is due to the short nucleation zone. As most droplets contributing to the reversal of subcooling are nucleated over a short distance, they exhibit similar growth with similar asymptotic radii.

The similarity between the droplet spectra is indicative of a similar cumulative release of latent heat over the whole nozzle with the heat-transfer-based models. In contrast, Hertz–Knudsen is influenced more by the change in humidity, with the larger partial pressure of the water vapor and the smaller amount of inert gas increasing the droplet growth.

Finally, the modification of Young's growth law only alters the predicted spectra slightly. The discrepancies to the original model can likely be attributed to numerical uncertainty or the binning process.

The analytical model allows a closer examination of the behavior of the growth models under the same conditions as in SUT43. Figure 13 shows the influence of the Knudsen number on the droplet growth rate at different radii. The direct increase of the Knudsen number with smaller radii leads to the visible shift of the curves as a whole. Again, the approach towards an almost constant growth rate in the continuous regime becomes visible with the heat-transfer-based models. The growth rate predicted with Hertz–Knudsen, however, continues to increase, even in the continuous regime. As Hertz–Knudsen is fully based on the molecular kinetic theory, it is invalid at these Knudsen numbers. At larger Knudsen numbers, the growth rate predicted by Hertz–Knudsen falls between Young and Gyarmathy, indicating that identical predictions as with Hertz–Knudsen can be achieved with Young by adjusting α.

Since Hertz–Knudsen does not take into account the droplet radius, while the growth rate predicted by heat-transfer-based models assumes a maximum at medium droplet radii, a shift between the curves in Fig. 13 relative to each other is visible. At radii close to the critical radius, the Hertz–Knudsen generally predicts larger values in comparison with heat-transfer-based models if the mass fraction of water vapor remains constant. However, condensation reduces the H_2O mass fraction available for droplet growth in the flows of humid air. The result of this reduction on the growth rate predicted by Young and Gyarmathy is shown in Fig. 14. Since the effect is similar for all heat-transfer-based models, only Young with $\alpha = 11$ is shown. While some influence

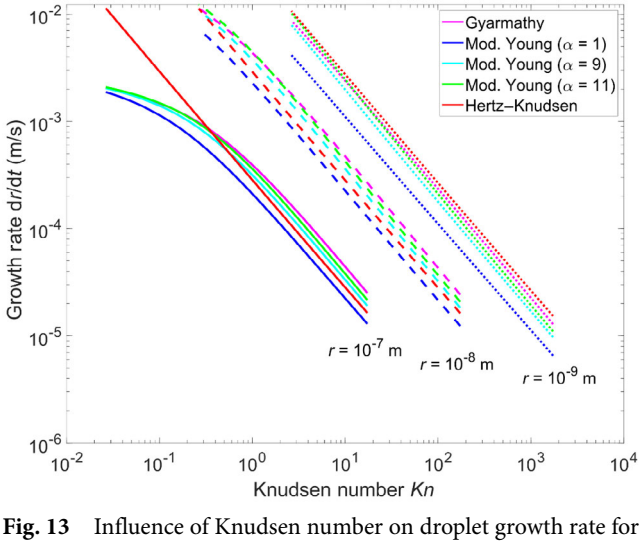

Fig. 13 Influence of Knudsen number on droplet growth rate for different growth laws with a constant subcooling of 30 K and $w_{H_2O} = 0.008$.

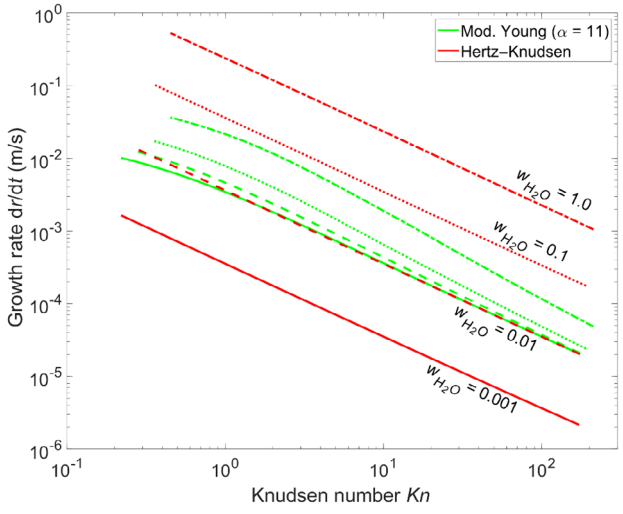

Fig. 14 Influence of mass fraction of water vapor w_{H_2O} in dependence of Knudsen number on droplet growth rate with Young and Hertz–Knudsen at $r = 10$ nm.

on Young is visible, the sensitivity of Hertz–Knudsen to changes in humidity is far larger. Furthermore, the reduction in growth rate with both models is disproportionate and their decrease follows exponential functions, with Young exhibiting a quicker decrease in growth rate than Hertz–Knudsen. This further explains the better accuracy of Hertz–Knudsen in humid air compared to heat-transfer-based models. As the reduction of the H_2O mass fraction is not fully reflected in the latter, they tend to overestimate condensation in flows with small mass fractions of water vapor and longer condensation zones, such as in SUT43. The former, on the other hand, can only be adapted empirically to a limited extent and loses its validity in transition and continuous regimes.

5 Conclusions

This investigation analyzed the accuracy of different growth laws for the prediction of condensation in nozzle flows of humid air at different Knudsen numbers. The Hertz–Knudsen model based on molecular kinetic theory was compared against the heat-transfer-based models by Gyarmathy and Young. Additionally, Young's growth model was adapted to be valid in humid air and other mixtures. The correction leads to a slight reduction in droplet growth rate with smaller mass fractions of water vapor, and produces results identical to the original equation in pure steam. CFD simulations of nozzle test case 252 by Moses and Stein (1978) and two cases at different humidity values by the Silesian University of Technology were conducted with an Euler–Lagrange approach in Ansys Fluent. A mesh convergence study showed a stronger sensitivity of the droplet spectra than of the pressure to the resolution of the mesh.

Generally, lower temperatures increase the subcooling and shift the onset of condensation upstream. This reduces the maximum Knudsen number, as the pressure is still larger at the Wilson point. In turn, the nucleation and droplet growth rates increase, and the subcooling is reversed over a shorter distance.

In flows with pure steam, Hertz–Knudsen was observed to greatly overestimate condensation. Heat-transfer-based models on the other hand provide good accuracy if the empirical tuning factors are adjusted accordingly. In contrast, condensation in flows of humid air is better predicted with molecular-kinetic growth laws, as they are more sensitive to the decrease in growth rate as a result of the reduction in H_2O mass fraction due to condensation. This is particularly evident in flows with longer condensation zones, i.e., in flows without condensation shocks. In the latter case, the initial nucleation and growth rates are sufficiently large to release enough latent heat. Thus, droplets nucleated later at lower H_2O mass fractions have virtually no impact on the release of latent heat, leading to similar predictions with all growth laws.

The correction of Young's growth law was shown to be too small to significantly impact accuracy. Since Young's growth law provides the highest fidelity and is valid with all Knudsen numbers, it provides a good basis for further adjustments. Future investigations should thus focus on adapting this law to fully incorporate changes in humidity into the adjusted heat transfer coefficient, which provides the basis for Young's growth law.

Finally, the accuracy of condensation models is still severely limited by the available validation data. Measurements of droplet radii in condensation of humid air, in particular, are virtually non-existent. As the transonic nozzles used for validation usually operate at low temperatures, comparability with applications at higher temperatures, such as turbines in fuel cell turbochargers, is not necessarily given. This should be addressed in future publications.

Acknowledgements

The authors thank the organizers of the International Wet Steam Modeling Project for granting access to the test cases and results of the project.

Funding note

Open Access funding enabled and organized by Projekt DEAL.

Declaration of competing interest

The authors have no competing interests to declare that are relevant to the content of this article.

References

Adam, S. 1996. Numerical and experimental investigation of unsteady nozzle flows with energy supply by homogeneous condensation. Ph.D. Dissertation. Karlsruhe, Germany: Karlsruhe Institute of Technology. Available at http://worldcatlibraries.org/wcpa/oclc/258359575.

Bakhtar, F. 2004. Special issue on wet steam. *Proceedings of the Institution of Mechanical Engineers, Part C: Journal of Mechanical Engineering Science*, 218: i–iii.

Bakhtar, F., Young, J. B., White, A. J., Simpson, D. A. 2005. Classical nucleation theory and its application to condensing steam flow calculations. *Proceedings of the Institution of Mechanical Engineers, Part C: Journal of Mechanical Engineering Science*, 219: 1315–1333.

Brent, R. P. 1973. *Algorithms for Minimization without Derivatives*. Englewood Cliffs, NJ, USA: Prentice-Hall.

Chambre, P. A., Schaaf, S. A. 2017. *Flow of Rarefied Gases*. Princeton, NJ, USA: Princeton University Press.

Chandler, K., White, A., Young, J. 2014. Non-equilibrium wet-steam calculations of unsteady low-pressure turbine flows. *Proceedings of the Institution of Mechanical Engineers, Part A: Journal of Power and Energy*, 228: 143–152.

Cunningham, E. 1910. On the velocity of steady fall of spherical particles through fluid medium. *Proceedings of the Royal Society of London, Series A*, 83: 357–365.

Dykas, S., Majkut, M., Smołka, K. 2020. Influence of air humidity on transonic flows with weak shock waves. *Journal of Thermal Sciences*, 29: 1551–1557.

Dykas, S., Majkut, M., Smołka, K., Strozik, M. 2017. Comprehensive investigations into thermal and flow phenomena occurring in the atmospheric air two-phase flow through nozzles. *International Journal of Heat and Mass Transfer*, 114: 1072–1085.

Dykas, S., Majkut, M., Smołka, K., Strozik, M. 2018. Numerical analysis of the impact of pollutants on water vapour condensation in atmospheric air transonic flows. *Applied Mathematical Computation*, 338: 451–465.

Fakhari, K. 2006. Development of a two-phase Eulerian–Lagrangian algorithm for condensing steam flow. In: Proceedings of the 44th AIAA Aerospace Sciences Meeting and Exhibit, 597.

Frenkel, Y. I. 1955. *Kinetic Theory of Liquids*. New York: Dover. Available at https://cds.cern.ch/record/106808?ln=de.

Gerber, A. G. 2002. Two-phase eulerian/Lagrangian model for nucleating steam flow. *Journal of Fluids Engineering*, 124: 465–475.

Gerber, A. G., Kermani, M. J. 2004. A pressure based Eulerian–Eulerian multi-phase model for non-equilibrium condensation in transonic steam flow. *International Journal of Heat and Mass Transfer*, 47: 2217–2231.

Grübel, M., Starzmann, J., Schatz, M., Eberle, T., Vogt, D. M., Sieverding, F. 2015. Two-phase flow modeling and measurements in low-pressure turbines—Part I: Numerical validation of wet steam models and turbine modeling. *Journal of Engineering for Gas Turbines and Power*, 137: 042602.

Gyarmathy, G. 1962. Grundlagen einer Theorie der Nassdampfturbine. Ph.D. Dissertation. Zürich, Switzerland: ETH Zurich. Available at https://www.research-collection.ethz.ch/handle/20.500.11850/131597.

Hill, P. G. 1966. Condensation of water vapour during supersonic expansion in nozzles. *Journal of Fluid Mechanics*, 25: 593–620.

Hughes, F. R., Starzmann, J., White, A. J., Young, J. B. 2016. A comparison of modeling techniques for polydispersed droplet spectra in steam turbines. *Journal of Engineering for Gas Turbines and Power*, 138: 042603.

IAPWS G12-15. 2015. Guideline on Thermodynamic Properties of Supercooled Water. Available at http://www.iapws.org/relguide/Supercooled.html.

IAPWS R7-97. 2012. Revised Release on the IAPWS Industrial Formulation 1997 for the Thermodynamic Properties of Water and Steam. Available at http://www.iapws.org/relguide/IF97-Rev.html.

Kantrowitz, A. 1951. Nucleation in very rapid vapor expansions. *The Journal of Chemical Physics*, 19: 1097–1100.

Moore, M. J., Sieverding, C. H. 1976. *Two-Phase Steam Flow in Turbines and Separators: Theory, Instrumentation, Engineering*. Washington: Hemisphere Publishing Corp.

Moses, C. A., Stein, G. D. 1978. On the growth of steam droplets formed in a Laval nozzle using both static pressure and light scattering measurements. *Journal of Fluids Engineering*, 100: 311–322.

Roumeliotis, I., Mathioudakis, K. 2006. Analysis of moisture condensation during air expansion in turbines. *International Journal of Refrigeration*, 29: 1092–1099.

Sasao, Y., Miyake, S., Okazaki, K., Yamamoto, S., Ooyama, H. 2013. Eulerian–Lagrangian numerical simulation of wet steam flow through multi-stage steam turbine. In: Proceedings of the ASME Turbine Technical Conference and Exposition, 1–10. Available at https://asmedigitalcollection.asme.org/GT/proceedings/GT2013/55201/V05BT25A045/250299.

Schiller, L. Naumann, A. 1935. A drag coefficient correlation. *Zeitschrift des Vereins Deutscher Ingenieure*, 77: 318–320.

Schuster, S., Brillert, D., Benra, F. K. 2018a. Condensation in radial turbines—Part I: Mathematical modeling. *Journal of Turbomachinery*, 140: 101001.

Schuster, S., Brillert, D., Benra, F. K. 2018b. Condensation in radial turbines—Part II: Application of the mathematical model to a radial turbine series. *Journal of Turbomachinery*, 140: 101002.

Starzmann, J., Schatz, M., Casey, M. V., Mayer, J. F., Sieverding, F. 2012. Modelling and validation of wet steam flow in a low pressure steam turbine. In: Proceedings of the ASME 2011 Turbo Expo: Turbine Technical Conference and Exposition, 2335–2346.

Starzmann, J., Hughes, F. R., Schuster, S., White, A. J., Halama, J., Hric, V., Kolovratník, M., Lee, H., Sova, L., Šťastný, M., et al. 2018. Results of the international wet steam modeling project. *Proceedings of the Institution of Mechanical Engineers, Part A: Journal of Power and Energy*, 232: 550–570.

Subramaniam, S. 2013. Lagrangian–Eulerian methods for multiphase flows. *Progress in Energy and Combustion Science*, 39: 215–245.

White, A. J. 2003. A comparison of modelling methods for polydispersed wet-steam flow. *International Journal of Numerical Methods in Engineering*, 57: 819–834.

Wiśniewski, P., Dykas, S., Yamamoto, S. 2020a. Importance of air humidity and contaminations in the internal and external transonic flows. *Energies*, 13: 3153.

Wiśniewski, P., Dykas, S., Yamamoto, S., Pritz, B. 2020b. Numerical approaches for moist air condensing flows modelling in the transonic regime. *International Journal of Heat and Mass Transfer*, 162: 120392.

Wiśniewski, P., Majkut, M., Dykas, S., Smołka, K., Zhang, G., Pritz, B. 2022a. Selection of a steam condensation model for atmospheric air transonic flow prediction. *Applied Thermal Engineering*, 203: 117922.

Wiśniewski, P., Zhang, G., Dykas, S. 2022b. Numerical investigation of the influence of air contaminants on the interfacial heat transfer in transonic flow in a compressor rotor. *Energies*, 15: 4330.

Wittmann, T., Bode, C., Friedrichs, J. 2021a. The feasibility of an Euler–Lagrange approach for the modeling of wet steam. *Journal of Engineering for Gas Turbines and Power*, 143: 041004.

Wittmann, T., Lück, S., Bode, C., Friedrichs, J. 2021b. Modelling the condensation phenomena within the radial turbine of a fuel cell turbocharger. *International Journal of Turbomachinery, Propulsion and Power*, 6: 23.

Wittmann, T., Lück, S., Hertwig, T., Bode, C., Friedrichs, J. 2021c. The influence of condensation on the performance map of a fuel cell turbocharger turbine. In: Proceedings of the ASME Turbomachinery Technical Conference and Exposition, 1–12.

Wróblewski, W., Dykas, S., Gepert, A. 2009. Steam condensing flow modeling in turbine channels. *International Journal of Multiphase Flow*, 35: 498–506.

Young, J. B. 1982. Spontaneous condensation of steam in supersonic nozzles. *Physicochemical Hydrodynamics*, 3: 57–82. Available at https://ntrl.ntis.gov/NTRL/dashboard/searchResults/titleDetail/N8113306.xhtml.

Young, J. B. 1995. Condensation in jet engine intake ducts during stationary operation. *Journal of Engineering for Gas Turbines and Power*, 117: 227–236.